We thank the anonymous reviewer for their kind words, as well as their thorough feedback and useful suggestions, which helped improve our manuscript. Our replies to the reviewer's comments *are written in blue italics. Proposed changes to the manuscript are highlighted in red.*

As for the water (and latent heat) fluxes issue, the authors invested a lot of efforts to look for reasons with different stomatal conductance models and water uptake functions. I think an expanded discussion about the interactions between vegetation settings from the LPJ-GUESS model and physical environments derived from the new biophysical processes would be helpful. This would also be helpful for understanding the differences in productivity between the original LPJ-GUESS and it coupled with LSM.

LPJ-GUESS calculates many vegetation properties dynamically, including key photosynthetic quantities such as Vmax. The new scheme interacts with these processes, and changes in simulated fluxes and productivity arise as a result of the interplay of many factors. We found that the biggest discrepancies between the standard model and the LSM version are due to the latter using leaf temperature, rather than daily averaged air temperature, for photosynthetic calculations. Leaf temperature can be several degrees above air temperature, affecting the photosynthetic rate directly, via the temperature inhibition factor, but also (and most dramatically in the case of C4 grasses) indirectly, by mitigating nitrogen limitation of photosynthesis. This is seen in simulations where we restrict establishment to grassy PFTs and C4 grasses emerge as the dominant grass type. While this effect seems to be far less pronounced in a potential natural vegetation simulation, due to trees entering the competition, it may be important when simulating C4 crops (since these grow without competition in well-watered conditions). The effect of leaf temperature on the biochemical nitrogen limitation of photosynthesis, and how it affects C4 grass productivity in competition and no-competition situations, is discussed in detail in section 4.2.

We now discuss in the supplement how the new simulated physical environments affect soil carbon and nitrogen build-up and how the PAR absorption calculations compare for the old and the new schemes (see attached document). We also discuss how the different stomatal conductance and soil water uptake formulations lead to differences in simulated soil water content that can alter the PFT composition (new section 3.4.4, attached).

We also suggest adding the following text to sect. 3.4.2:

"The above-described discrepancies between standard LPJ-GUESS and the LSM versions stem from the different physical environments simulated in the models. Calculating assimilation at the newly simulated canopy temperature, rather than the air temperature, can lead to either higher or lower productivity, depending on the optimal photosynthetic temperature ranges of each PFT and the impact of temperature on nitrogen limitation (Sec. 4.2). Canopy temperature also affects autotrophic respiration, while differences in the simulated soil humidity and temperature impact organic matter decomposition rates and heterotrophic respiration. The combination of these effects results in differences in simulated carbon and nitrogen pools and NEE (we have included a comparison between soil carbon and nitrogen pools simulated by standard LPJ-GUESS and LPJ-GUESS/LSM in the supplement)."

We will now address the minor comments.

1. Line 146: the unit of lambda. I think "C-1" is not necessary. The number of 2.44x10^6 has included an assumption of normal water temperature

We thank the reviewer for spotting the mistake in the units. Lambda represents the amount of energy that it takes to evaporate a unit mass of liquid water, so the correct units should be of energy per unit mass (J/kg). We will correct the text accordingly.

2. Lines 380 and 388: How do the vegetation conditions vary with the actual vegetation? I think the vegetation and soil states (equilibrium or not) may affect NEE, as shown in Fig. 14 that the simulations are close to equilibrium state.

4. Lines 572: measured NEE is more negative than those simulated. I think it is related to how far the vegetation is from its theoretical equilibrium state. Disturbances also play a role here. For example, at equilibrium state, an ecosystem will have a zero NEE (or fluctuated around zero) if the system has no disturbances. However, if it is equilibrated with a particular disturbance regime (e.g., a given fire frequency distribution), the system must have a negative NEE that is to counter the carbon release at disturbance events. In long-term, it is still carbon neutral. This is the pattern this paper showed in this section that observations have higher carbon sink (more negative NEE) than the simulated (with 500 years of model run).

We agree with the reviewer that the discrepancy in NEE probably reflects the fact that the simulated carbon pools are close to equilibrium with the synthetic climate data used to spin up the model, and that this set up differs from the actual situation at the different sites (this is seen also in the difference between the variabilities of observed and simulated fluxes). In a standard LPJ-GUESS simulation, the spinup procedure is designed to bring carbon pools close to equilibrium with pre-industrial conditions, before simulating the historical period of rising temperatures and CO2 concentrations. Here, our primary goal was to evaluate the sub-daily latent and sensible heat fluxes calculated by the augmented model against observations, and then compare the ecosystem-related predictions (structure, composition and fluxes) of the new LSM model with those made by the standard (non-LSM) version. Therefore, differences between simulated and measured NEE are to be expected because we did not attempt to fully reproduce or account for site history, including age, disturbance, and legacies arising from historical trends in CO2 concentration. Evaluating simulated ecosystem productivity and carbon fluxes against observations, as well as the differences between the standard and the augmented model in regional and global scales, is the object of future work, but was out of the scope of this paper.

We suggest adding the following sentence in section 3.4.4:

"These discrepancies between observed and simulated NEE magnitude and variability reflect the fact that, in the simulations, the carbon pools are all close to equilibrium with the climate and atmospheric CO2 concentration as a result of the spinup procedure described in section 3.2. Differences are to be expected because we did not attempt to fully reproduce or account for site history, including age, disturbance, and legacies arising from historical trends in CO2 concentration."

Additionally, we added a discussion of the build-up of soil organic matter pools during the spinup phase in the supplement.

3. Line 506 section Ecosystem structure and function: They are related to the settings of the vegetation model since the structure is highly dynamic. How to make them consistent with each case and the measurement data?

For this work, we used the standard set of PFTs provided with LPJ-GUESS, which aims to capture the main functional traits of different vegetation classes in global simulations. Our aim in this paper was to evaluate how well the model (including the standard set of PFTs) simulated energy fluxes, rather than fitting the PFT parameters at each site specifically to achieve a best fit between model and observations. We chose this approach since the end goal is to perform regional and global runs. Also, see response to previous comment.

5. Time steps of and growth (yearly) and SOM (daily): how LAI dynamics and heterotrophic respiration are calculated? Usually, LAI should be updated daily and Rh hourly (or half hourly). Are they connected with plant growth and SOM dynamics at each step, respectively? This just need to clarify. I may miss the description.

- In this work we did not modify the original model's growth and phenology routines. At present, the allocation of carbon to the different plant structures (what we call growth) is simplified in the model, happening annually. The phenological status is calculated and updated daily according to the phenology of the different PFTs (Raingreen, Summergreen, Evergreen, as described in appendix B4 of Smith et al. (2014), https://doi.org/10.5194/bg-11-2027-2014). This is stated at the beginning of section 2.2 of the model description and in Figure 1.

- Rh is updated daily in the current version of the model. Even though Rh can vary on diurnal timescales, we focused on averages of yearly NEE over the measuring period, so we assumed calculating Rh on a daily basis was sufficient for our purposes. We stress, however, that photosynthesis and autotrophic respiration are calculated on a subdaily basis, consistent with the canopy energy balance, and accumulated to calculate daily NPP, and then subtracted from daily RH to calculate daily NEE at the end of the day. To clarify this, we added the following text at the beginning of section 2.2.4:

"The net photosynthetic assimilation is accumulated over the diurnal cycle and subtracted from heterotrophic respiration (Rh, computed daily) to calculate daily net ecosystem exchange (NEE)."

6. In discussion, for the water uptake functions and C4 grass carbon assimilation simulations, they are phenomenological equations in the model that directly link soil water availability to leaf functions. A discussion of actual plant-soil hydraulics would be helpful for understanding why they happen and why we don’t have to spend much time to tune these functions.

We agree with the reviewer that these expressions are oversimplifications of the very complex process of stomatal regulation. To stress this fact in a concise way, we suggest adding the following text when introducing the soil moisture stress factor (end of section 2.2.4):

"This type of formulations, which are widely use in LSMs (see Damour et al, 2010, for an overview), are phenomenological relationships that attempt to capture the response of plants to water stress in a rather simplified way (Egea et al., 2011; De Kauwe et al., 2013). Transpiration of soil water by plants is primarily driven by the water potential gradient along the soil-plant-atmosphere continuum. Plants regulate this gradient by opening and closing their stomata in response to environmental factors, including leaf water potential, vapor pressure deficit, and soil water availability, in a way that depends on their hydraulic strategy (a detailed discussion can be found in Lambers et al, 2008). Including a more explicit representation of soil-plant-air hydraulics as well as physiological constraints in a stomatal conductance model has been shown to perform better than the above formulations under soil water stress conditions (Bonan et al., 2014). However, implementing these more complex models in

ESMs remains a challenge due to a lack of data for broader applicability and computational efficiency tradeoffs (Clark et al., 2015)."

References:

Bonan, G. B., Williams, M., Fisher, R. A., & Oleson, K. W. (2014). Modeling stomatal conductance in the earth system: Linking leaf water-use efficiency and water transport along the soil–plant–atmosphere continuum. Geoscientific Model Development, 7(5), 2193–2222. https://doi.org/10.5194/gmd-7-2193-2014

Damour, G., Simonneau, T., Cochard, H., & Urban, L. (2010). An overview of models of stomatal conductance at the leaf level. Plant, Cell & Environment, 33(9), 1419–1438. https://doi.org/10.1111/j.1365-3040.2010.02181.x

De Kauwe, M. G., Kala, J., Lin, Y.-S., Pitman, A. J., Medlyn, B. E., Duursma, R. A., Abramowitz, G., Wang, Y.-P., & Miralles, D. G. (2015). A test of an optimal stomatal conductance scheme within the CABLE land surface model. Geoscientific Model Development, 8(2), 431–452. https://doi.org/10.5194/gmd-8-431-2015

Egea, G., Verhoef, A., & Vidale, P. L. (2011). Towards an improved and more flexible representation of water stress in coupled photosynthesis–stomatal conductance models. Agricultural and Forest Meteorology, 151(10), 1370–1384. https://doi.org/10.1016/j.agrformet.2011.05.019

Lambers, H., Chapin, F. S., & Pons, T. L. (2008). Plant Physiological Ecology. Springer New York. https://doi.org/10.1007/978-0-387-78341-3

Clark, M. P., Fan, Y., Lawrence, D. M., Adam, J. C., Bolster, D., Gochis, D. J., Hooper, R. P., Kumar, M., Leung, L. R., Mackay, D. S., Maxwell, R. M., Shen, C., Swenson, S. C., & Zeng, X. (2015). Improving the representation of hydrologic processes in Earth System Models. Water Resources Research, 51(8), 5929–5956. https://doi.org/10.1002/2015WR017096

7. I just realized the codes of LPJ-GUESS are still not publicly available. Maybe, this question should be asked by the handling editor. Does it comply with the journal's policy?

As specified in the "Code availability section" of the manuscript, "The [LPJ-GUESS] source code can be made available with a collaboration agreement under the acceptance of certain conditions. For this reason, a DOI for the model code cannot be provided. The code with the augmentations developed for this paper is available to the editor and reviewers via a restricted link, on the condition that the code is used only for review purposes, and is deleted after the review process." In any case, we are happy to provide the code upon request.

This is consistent with point #2 in the core principles of the journal's code and data policy (https://www.geoscientific-model-development.net/policies/code_and_data_policy.html):

"Where the authors cannot, for reasons beyond their control, publicly archive part or all of the code and data associated with a paper, they must clearly state the restrictions. They must also provide confidential access to the code and data for the editor and reviewers in order to enable peer review. The arrangements for this access must not compromise the anonymity of the reviewers. All manuscripts

which do not make code and data available at this level are to be rejected. Where only part of the code or data is subject to these restrictions, the remaining code and/or data must still be publicly archived. In particular, authors must make every endeavour to publish any code whose development is described in the manuscript."

NEW SECTION 3.4.1

3.4 Results

3.4.1 Ecosystem composition and function

The emerging ecosystem composition in both LSM runs is similar to the standard LPJ-GUESS prediction over forests and grasslands, but it is sensitive to the choice of stomatal conductance scheme at some savanna and woody savanna sites, and at ZM-Mon (Table 3). Figure 7 shows the LAI evolution of the established PFTs over the spinup period for the CLM/BB, CLM/Med and standard LPJ-GUESS simulations at three selected sites. All three simulations predict a C_4 grassland at PA-SPs, but LAI values are much higher in the LSM simulations (~ 11) than the LPJ-GUESS prediction (~ 6.5). At BR-Sa1 (a tropical rainforest), the species composition is similar for the three simulations, but LAI values are lower in the LSM runs (~ 5.5 vs ~ 6.2). At AU-Dry, the use of different stomatal conductance schemes causes a shift in PFT composition. The BB simulation favors evergreen trees, while the PFT mix is dominated by raingreen trees in the Med simulation, a prediction closer to standard LPJ-GUESS. We found this behaviour to be representative of how the soil water uptake response factor and the stomatal conductance scheme influence the PFT composition at most savanna and woody savanna sites in the LSM simulations. A stronger limitation on transpiration (e.g. the NOAH-type water uptake response factor or the Ball-Berry stomatal conductance model) results in higher soil water content throughout the year, which promotes stronger growth of evergreen trees.

Model predictions for the rest of the selected variables are shown in Table 4. The two C_3 grassland sites show different behaviour with respect to ecosystem productivity and respiration. At AU-Emr, LSM simulations predict substantially lower gross primary production (GPP) and autotrophic respiration (R_a) than standard LPJ-GUESS, which results in lower estimates of net primary production (NPP). This site is a net carbon source (positive NEE) in all three simulations, which agrees with observations. At ES-Amo, the NPP increase in the LSM runs is larger than the decrease in heterotrophic respiration (R_h), resulting in an enhanced carbon sink compared to standard LPJ-GUESS.

At PA-SPn, both NPP and R_h decrease in the LSM simulations, but the former decreases less than the latter, resulting in slightly weaker carbon sinks in the LSM simulations. The three simulations predict carbon fluxes much smaller than the measured value of $-458\,\mathrm{gC}^{-2}\mathrm{y}^{-1}\mathrm{m}^{-2}$. Predictions for ZM-Mon show some differences between runs, but NPP and R_h are similar in all three simulations, resulting in carbon sinks of $\sim -62\,\mathrm{gC}^{-2}\mathrm{y}^{-1}\mathrm{m}^{-2}$. This result is inconsistent with measurements at the site, which indicate a carbon source of $143\,\mathrm{gC}^{-2}\mathrm{y}^{-1}\mathrm{m}^{-2}$.

Differences in simulated carbon fluxes between standard LPJ-GUESS and the CLM/BB and CLM/Med runs for the remaining land cover types are summarized in Fig. 8. Both LSM runs predict, on average, higher GPP and R_a values than the non-LSM simulation over C_4 grasslands, savanna and woody savanna sites. This results in an increased average NPP value in C_4 grasslands ($\sim 18\%$ in the CLM/BB run and $\sim 31\%$ in the CLM/Med run), and a decreased average NPP at woody savanna sites ($\sim -11\%$ and $\sim -7\%$ in the CLM/BB and the CLM/Med runs, respectively). At savanna sites, the increase in GPP in both LSM simulations is similar ($\sim 10\%$), but the increase in R_a is much higher for CLM/BB, which leads to changes in NPP of $\sim -10\%$ in the CLM/BB run and $\sim 6\%$ in the CLM/Med run. At forest sites, the balance between decreased values of GPP and R_a results in lower NPP values in the LSM simulations. Average values of R_h in the CLM/BB simulation increase over C_4 grasslands, and decrease over woody savannas and evergreen forests. The CLM/Med simulation shows the same pattern except

Site	TeBE			TrBR			TrIBE			TrBE			C3G			C4G		
	LPJ-G	BB	Med	LPJ-G	BB	Med	LPJ-G	BB	Med	LPJ-G	BB	Med	LPJ-G	BB	Med	LPJ-G	BB	Med
AU-Emr	–	–	–	–	–	–	–	–	–	–	–	–	**61**	**23**	**24**	–	–	–
ES-Amo	–	–	–	–	–	–	–	–	–	–	–	–	**62**	**68**	**61**	–	–	–
AU-DaP	–	–	–	–	–	–	–	–	–	–	–	–	–	–	–	**93**	**96**	**97**
AU-Stp	–	–	–	–	–	–	–	–	–	–	–	–	–	–	–	**77**	**57**	**61**
CG-Tch	–	–	–	–	–	–	–	–	–	–	–	–	1	–	–	**89**	**98**	**98**
PA-SPs	–	–	–	–	–	–	–	–	–	–	–	–	–	–	–	**95**	**98**	**98**
AU-DaS	–	–	–	5	**53**	24	2	13	11	**58**	4	**39**	–	–	–	18	8	13
AU-Dry	–	–	–	4	**50**	14	2	13	5	**45**	2	**45**	–	–	–	26	7	20
SD-Dem	–	–	–	1	9	–	–	4	–	18	**16**	9	–	–	–	**27**	13	**40**
AU-Ade	–	–	–	5	**51**	30	5	16	10	**52**	4	**32**	–	–	–	19	7	11
AU-Gin	**51**	**51**	**39**	–	–	–	–	–	–	–	–	–	6	1	5	–	–	–
AU-How	–	–	–	6	**55**	**42**	5	19	12	**57**	4	20	–	–	–	17	6	12
AU-RDF	–	–	–	6	**58**	31	1	16	11	**52**	4	**34**	–	–	–	21	3	7
AU-Rob	–	–	–	**60**	**62**	**57**	27	18	17	2	1	2	–	–	–	3	5	6
BR-Sa1	–	–	–	**68**	**63**	**67**	22	25	24	2	7	5	–	–	–	5	6	4
BR-Sa3	–	–	–	**61**	**62**	**63**	28	18	16	5	2	4	–	–	–	5	6	4
GF-Guy	–	–	–	**69**	**63**	**60**	22	22	19	2	3	4	–	–	–	2	6	8
GH-Ank	–	–	–	**73**	**60**	**65**	19	18	16	2	6	8	–	–	–	2	4	5
MY-PSO	–	–	–	**74**	**64**	**64**	20	15	13	3	7	8	–	–	–	4	6	8
PA-SPn	–	–	–	**67**	**59**	**62**	28	22	18	3	4	6	–	–	–	3	8	7
ZM-Mon	–	–	–	3	**40**	11	2	10	4	**60**	19	**49**	–	–	–	12	7	13

Table 3. Foliar projective cover, averaged over the whole simulated period, of the plant functional types predicted for each site, given as a percentage. The LSM simulations use the CLM type water uptake response factor. The dominant PFT for each site is highlighted in bold font.

Site	LAI				GPP			Ra			NPP			Rh			NEE			
	Obs	LPJ-G	BB	Med	LPJ-G	BB	Med	LPJ-G	BB	Med	LPJ-G	BB	Med	LPJ-G	BB	Med	Obs	LPJ-G	BB	Med
AU-Emr	0.7	2.0	**0.6**	**0.6**	1190	**436**	413	927	**364**	329	263	72	**84**	305	**105**	93	53	**42**	32	11
ES-Amo	–	2.0	2.4	2.0	779	998	**819**	485	680	**522**	294	317	**297**	263	**258**	234	182	**−30**	−58	−62
Average	0.7	2.0	1.5	**1.3**	984	**717**	616	706	**522**	426	279	**194**	191	284	**182**	164	118	**6**	−13	−26
AU-DaP	1.5	**5.9**	7.2	8.0	1414	**1597**	1941	480	**648**	769	934	**950**	1171	792	**826**	1004	−210	−142	−123	**−167**
AU-Stp	0.5	3.3	**1.9**	2.2	975	555	**722**	365	217	**264**	610	337	**457**	564	302	**407**	−52	−46	−36	**−50**
CG-Tch	2.0	**4.7**	11.4	11.6	1064	**1970**	2024	351	**760**	783	712	**1210**	1242	624	**1094**	1121	−148	−88	−116	**−120**
PA-SPs	5.4	**6.6**	10.8	11.1	1454	**2038**	2111	538	**798**	828	915	**1240**	1284	842	**1146**	1181	277	**−74**	−95	−102
Average	2.4	**5.1**	7.8	8.2	1227	**1540**	1699	434	**606**	661	793	**934**	1038	706	**842**	929	−33	**−88**	−92	−110
AU-DaS	1.5	**3.0**	3.2	3.1	1094	1129	**1110**	480	607	**524**	614	522	**585**	521	458	**528**	−284	**−93**	−63	−57
AU-Dry	1.2	**2.5**	2.8	2.6	844	1019	**958**	357	554	**448**	487	**464**	**510**	446	381	**437**	−307	−40	**−83**	−73
SD-Dem	0.9	**1.2**	**1.2**	1.3	401	**413**	509	159	198	**184**	242	**216**	326	230	**196**	295	−73	−11	−20	**−31**
Average	1.2	**2.2**	2.4	2.3	780	**854**	859	332	453	**385**	448	401	**474**	399	345	**420**	−221	−48	**−56**	−54
AU-Ade	1.1	**3.0**	3.3	**3.0**	1067	1126	**1073**	471	617	**543**	596	510	**531**	580	482	**521**	−272	−14	**−28**	−10
AU-Gin	0.9	1.7	1.9	**1.6**	1168	1419	**1268**	932	1190	**1059**	238	**229**	210	256	**247**	228	−317	**17**	19	18
AU-How	1.5	**3.3**	3.7	3.5	1230	1258	**1245**	530	664	**627**	700	593	**618**	638	486	**552**	−692	−62	**−108**	−65
AU-RDF	1.6	**2.8**	3.6	3.1	990	1264	**1203**	441	737	**638**	550	527	**567**	562	**533**	634	329	11	6	**68**
Average	1.3	**2.7**	3.1	2.8	1114	1267	**1197**	593	802	**717**	521	465	**481**	509	437	**484**	−238	−12	**−28**	3
AU-Rob	4.3	4.8	4.9	**4.6**	1647	**1687**	1733	803	**841**	869	842	**847**	865	794	**808**	778	−744	−46	−39	**−86**
BR-Sa1	6.5	**6.3**	5.6	5.8	2359	1908	**2048**	1215	985	**1071**	1143	924	**977**	953	848	**857**	−4	−190	**−76**	−120
BR-Sa3	6.5	**4.8**	4.6	4.6	1692	1573	**1652**	865	830	**877**	827	743	**775**	732	635	**658**	−105	−94	**−108**	−116
GF-Guy	5.9	**5.4**	5.0	5.0	2034	1804	**1855**	1044	954	**972**	990	850	**883**	835	702	**806**	−157	**−155**	−147	−77
GH-Ank	–	5.7	4.8	5.1	1956	1614	**1707**	994	849	**888**	962	766	**820**	835	724	**749**	–	−126	−40	−70
MY-PSO	6.5	**6.1**	4.9	5.1	2279	1625	**1804**	1139	846	**950**	1140	778	**854**	974	684	**716**	−971	**−166**	−95	−138
Average	5.9	**5.5**	5.0	5.0	1994	1702	**1800**	1010	884	**938**	984	818	**862**	854	734	**761**	−396	**−130**	−84	−101
PA-SPn	2.9	5.3	**4.8**	4.9	1785	1578	**1654**	917	817	**854**	870	760	**799**	812	718	**757**	−458	**−59**	−42	−41
ZM-Mon	1.6	2.7	2.5	**2.4**	975	1061	**948**	394	498	**406**	580	**564**	542	523	**503**	476	143	**−58**	−60	−66
Average	2.3	4.0	**3.6**	**3.6**	1380	**1320**	1301	656	**658**	630	725	662	**671**	668	611	**617**	−157	**−58**	−51	−54

Table 4. Comparison of selected variables related to simulated ecosystem structure and function between standard LPJ-GUESS and the LSM version at the selected sites. The LSM values are from the CLM/BB and the CLM/Med simulations. Gross primary production (GPP), autotrophic respiration (Ra), net primary production (NPP), heterotrophic respiration (Rh) and net ecosystem exchange (NEE) are given in $\mathrm{gCm^{-2}y^{-1}}$. Bold fonts in the LAI and NEE columns indicate the closest match to the observed value. Bold fonts in the rest of the columns indicate the LSM prediction closest to standard LPJ-GUESS.

Table 5. List of Plant Functional Types in the standard configuration of LPJ-GUESS (only PFTs predicted by the simulations in this study are listed)

Plant functional type	Abbreviation
Temperate Broadleaf Evergreen	TeBE
Tropical Broadleaf Raingreen	TrBR
Tropical shade-Intolerant Broadleaf Evergreen	TrIBE
Tropical Broadleaf Evergreen	TrBE
C_3 Grass	C3G
C_4 Grass	C4G

over savanna sites, where R_{h} increases by $\sim 5\%$ with respect to standard LPJ-GUESS. Over woody savannas, the average NEE change is $\sim -129\%$ for the CLM/BB run, and $\sim 122\%$ for the CLM/Med run.

The above-described discrepancies between standard LPJ-GUESS and the LSM versions stem from the different physical environments simulated in the models. Calculating assimilation at the newly simulated canopy temperature, rather than the air temperature, can lead to either higher or lower productivity, depending on the optimal photosynthetic temperature ranges of each PFT and the impact of temperature on nitrogen limitation (Sec. 4.2). Canopy temperature also affects autotrophic respiration, while differences in the simulated soil humidity and temperature impact organic matter decomposition rates and heterotrophic respiration. The combination of these effects results in differences in simulated carbon and nitrogen pools and NEE (we have included a comparison between soil carbon and nitrogen pools simulated by standard LPJ-GUESS and LPJ-GUESS/LSM in the supplement).

The large relative changes in NEE between simulations result from small discrepancies in magnitude. Figure 9 shows a comparison between land-cover averages of measured and modeled NEE for C_4 grasslands, savanna, woody savanna and evergreen forests. Average measured NEE is negative for all land cover types, and substantially more negative than in the simulations for savanna, woody savanna and evergreen broadleaf forests, implying an average underestimation of the C sink by the models at these sites. At C_4 sites simulations predict NEE values between $-88\,\mathrm{gCm^{-2}y^{-1}}$ and $-110\,\mathrm{gCm^{-2}y^{-1}}$, while observations indicate a less negative value of $-33\,\mathrm{gCm^{-2}y^{-1}}$. For savanna, measured NEE is $-221\,\mathrm{gCm^{-2}y^{-1}}$, while simulations predict an average between $-48\,\mathrm{gCm^{-2}y^{-1}}$ and $-56\,\mathrm{gCm^{-2}y^{-1}}$. For woody savanna, measured NEE averages to $-238\,\mathrm{gCm^{-2}y^{-1}}$, while simulated fluxes range between $-28\,\mathrm{gCm^{-2}y^{-1}}$ and $3\,\mathrm{gCm^{-2}y^{-1}}$. Simulated fluxes at evergreen broadleaf forests are, on average, between -84 and $-130\,\mathrm{gCm^{-2}y^{-1}}$, while measurements indicate an average NEE of $-396\,\mathrm{gCm^{-2}y^{-1}}$. However, this is the result of very large negative values measured at AU-Rob and MY-PSO (Table 4). In general, differences in simulated fluxes between standard LPJ-GUESS and the LPJ-GUESS/LSM simulations are small compared to the magnitude of observed fluxes, and the interannual and cross-site variability of the measured fluxes is much greater than in the simulations. The discrepancies between observed and simulated NEE magnitude and variability reflect the fact that, in the simulations, the carbon pools are all close to equilibrium with the climate and atmospheric CO_2 concentration as a result of the spinup procedure de-

scribed in section 3.2. Differences between observed and simulated NEE values are to be expected because we did not attempt to reproduce site history, including age, disturbance, and legacies arising from historical trends in CO_2 concentration.

3.4.2 Annual and diurnal cycles of turbulent heat fluxes

Figure 10 shows examples of simulated and observed monthly averages of turbulent and latent heat fluxes over the course of a year at four sites: Gingin (AU-Gin), Daly River Savanna (AU-DaS), Santarem Km67 (BR-Sa1) and Guyaflux (GF-Guy). Examples of the monthly-averaged diurnal cycle for the same sites are shown in Figs. 11 and 12. We chose these sites and years to illustrate situations with varying degrees of agreement between simulations and measurements. The simulated fluxes are from the run using the CLM-type water uptake response function and the Medlyn model of stomatal conductance (CLM/Med).

At the AU-Gin site, the shape of the annual cycles of latent and sensible heat is well reproduced in the simulations (Fig. 10a). Sensible heat is largest at the beginning of the year, decreases steeply to its minimum around June-July, and starts increasing again around August. The simulation agrees well with measurements most of the year, but overestimates sensible heat by $\sim 45\,\mathrm{Wm^{-2}}$ in the first two months. Observed latent heat increases at the start of the wet season and dominates the turbulent exchange from May to September. Simulated latent heat is overestimated by up to $\sim 25\,\mathrm{Wm^{-2}}$ during the wet season, and underestimated in the dry season. The shift from larger sensible heat to larger latent heat in May is well captured in the simulation, but, due to the overestimation of latent heat, the shift back to larger sensible heat flux is delayed by about two months with respect to the observations. The average simulated diurnal cycle of sensible heat is overestimated in January, peaking at $\sim 700\,\mathrm{Wm^{-2}}$ (observed: $\sim 500\mathrm{Wm^{-2}}$), while it agrees very well with observations in May and September, both in terms of magnitude and day-to-day variability (Fig. 11a–c).

At the AU-DaS site (Fig. 10b), observed and simulated heat fluxes diverge substantially during the dry season (July-November). Simulated monthly averages of latent heat are $\sim$ 20–30 $\mathrm{Wm^{-2}}$ above measured values from March to May, and $\sim$ 30–45 $\mathrm{Wm^{-2}}$ below the measurements between August and October. The average simulated latent heat diurnal cycle peaks at $\sim 350\,\mathrm{Wm^{-2}}$ in May (observed: $\sim 175\,\mathrm{Wm^{-2}}$), and at $\sim 25\,\mathrm{Wm^{-2}}$ in September (observed: $\sim 145\,\mathrm{Wm^{-2}}$; Fig. 11j–l). This marked divergence from measured values happens in very dry periods, when the simulated soil moisture in the rooting zone drops close to the wilting point and there is not enough precipitation to replenish it until the start of the wet season. As a consequence, sensible heat is greatly overestimated. Simulated monthly averages rise sharply and peak at $\sim$ 120–140 $\mathrm{Wm^{-2}}$ from September to October, while measured values stay at $\sim 60\,\mathrm{Wm^{-2}}$ throughout the dry season. The average sensible heat diurnal cycle peaks at $\sim 530\,\mathrm{Wm^{-2}}$ in September, while the observed average diurnal peak is slightly under $\sim 300\,\mathrm{Wm^{-2}}$ (Fig. 11g–i).

Monthly averages of sensible and latent heat at the BR-Sa1 tropical rainforest site show little variability throughout the year (Fig. 10c). Measured sensible heat flux stays at $\sim 20\,\mathrm{Wm^{-2}}$ for most of the year, and increases to $\sim 30\,\mathrm{Wm^{-2}}$ around August and September, when measured precipitation reaches its minimum. During this period, the soil retains enough moisture in the rooting zone to maintain average latent heat levels at $\sim$ 80–90 $\mathrm{Wm^{-2}}$. Sensible and latent heat fluxes are systematically overestimated by the model by $\sim$ 10–20 $\mathrm{Wm^{-2}}$. This overestimation takes place even when simulated net radiation is very close to observations (June to November), so, assuming the measurements do not underestimate the fluxes, it must be compensated by

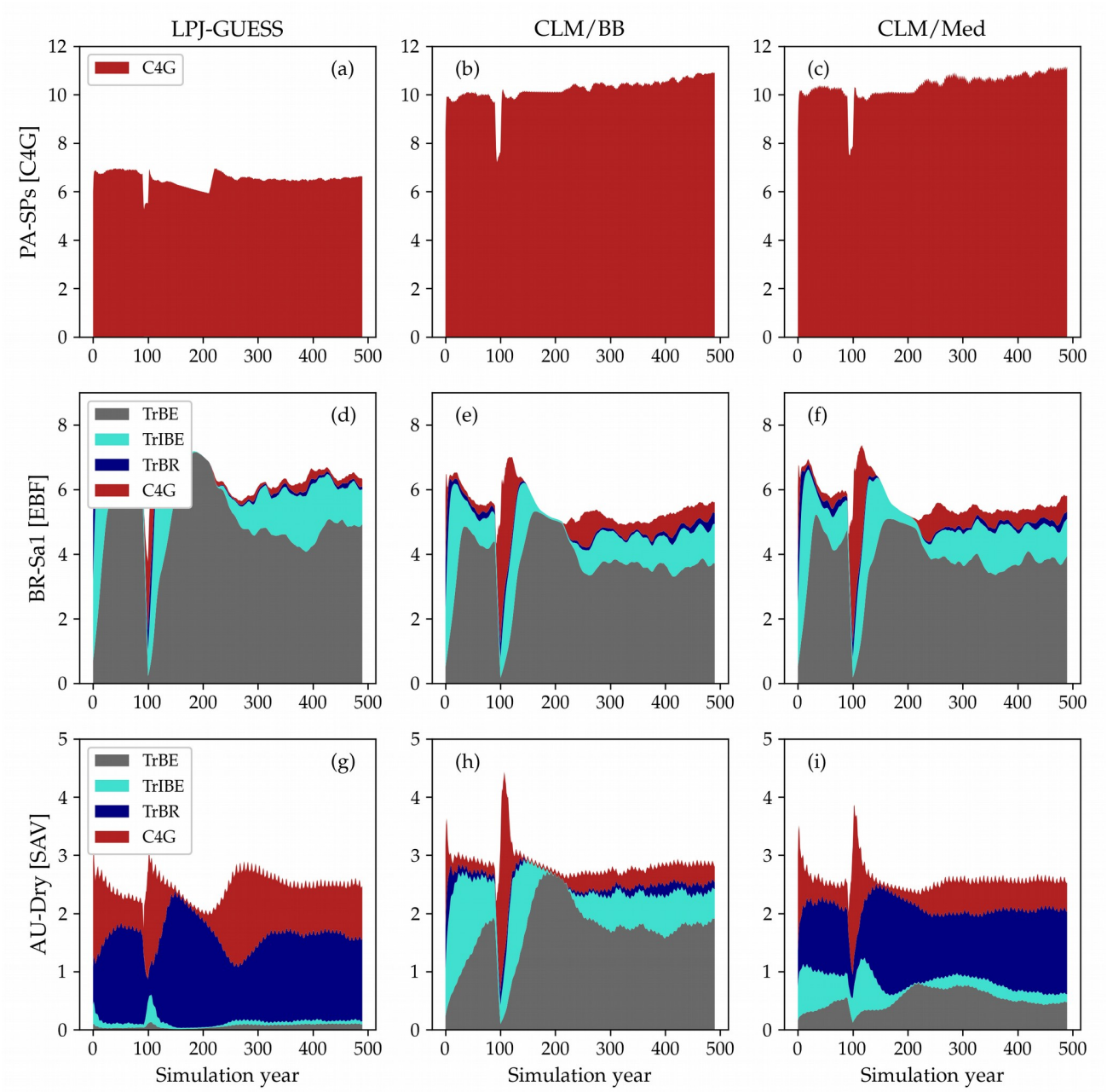
LPJ-GUESS
CLM/BB
CLM/Med
PA-SPs [C4G]
BR-Sa1 [EBF]
AU-Dry [SAV]
C4G
TrBE
TrIBE
TrBR
(a)
(b)
(c)
(d)
(e)
(f)
(g)
(h)
(i)
Simulation year

SUPPLEMENT

	LAI (obs)	LAI (mod)	PAR (LPJ-G)	PAR (LPJ-G/LSM)	% Change
AU-Emr	0.7	0.6	426	651	53.4
ES-Amo	-	2.1	708	928	32.1
AU-DaP	1.5	7.9	1839	1959	6.5
AU-Stp	0.5	2.2	607	774	28.6
CG-Tch	2.0	11.6	1925	1994	3.6
PA-SPs	5.4	11.1	1986	2076	4.5
AU-DaS	1.5	3.0	2150	2450	14.1
AU-Dry	1.2	2.6	1837	2183	18.9
SD-Dem	0.9	1.3	456	664	45.6
AU-Ade	1.1	3.0	2157	2460	14.1
AU-Gin	0.9	1.5	1553	2010	29.5
AU-How	1.5	3.4	2403	2634	9.7
AU-RDF	1.6	3.2	2283	2527	10.7
AU-Rob	4.3	4.9	2378	2430	2.2
BR-Sa1	6.5	5.7	2463	2470	0.3
BR-Sa3	6.5	4.7	2102	2169	3.2
GF-Guy	5.9	5.2	2377	2419	1.8
GH-Ank	-	5.1	1843	1879	1.9
MY-PSO	6.5	5.3	2385	2415	1.3
PA-SPn	2.9	4.9	2079	2129	2.4
ZM-Mon	1.6	2.4	1314	1635	25.0

Table 1: Comparison of PAR absorbed by the vegetation, calculated using the new radiative transfer scheme and the PAR absorption scheme in standard LPJ-GUESS. Data are from the CLM/Med simulations described in the paper. PAR values are averages over the measurement period of the simulations, in MJ/year/m^2. The percent change is relative to the standard LPJ-GUESS run.

1 Differences in PAR absorption between LPJ-GUESS and LPJ-GUESS/LSM

Table 1 shows a comparison of average PAR absorption per unit LAI calculated by the new radiative transfer scheme and the PAR absorption algorithm in stadard LPJ-GUESS. The calculations were made in the CLM/Med simulation, i.e., PAR absorption is calculated with both schemes in the same modeled areas for the purpose of this comparison. In general, the new radiative transfer calculates higher absorbed PAR values than standard LPJ-GUESS at sites with low modeled LAI values, while both calculations yield similar results at sites with high LAI values. This behaviour can be understood by examining PAR absorption by individual cohorts. Figure 1 shows PAR absorption by the vegetation over 60 years during the spinup period at BR-Sa1, starting after a disturbance. Three tree cohorts (0, 1 and 2) and a grass individual (4) establish. Initially, grass has a high LAI, but, as trees grow and the canopy thickens, the grass LAI declines (panels *c* and *d*). Calculated tree PAR absorption per leaf area is initially similar for both schemes (panel *a*), but as cohort 0 grows it shadows cohorts 1 and 2. The new radiative transfer scheme calculates lower PAR values for these two cohorts, but since their leaf area index is also declining, this does not contribute substantially to the overall difference, which is small and dominated by cohort 0 (panel *b*).

Figure 2 shows the same comparison for a patch at AU-Gin. In this case,

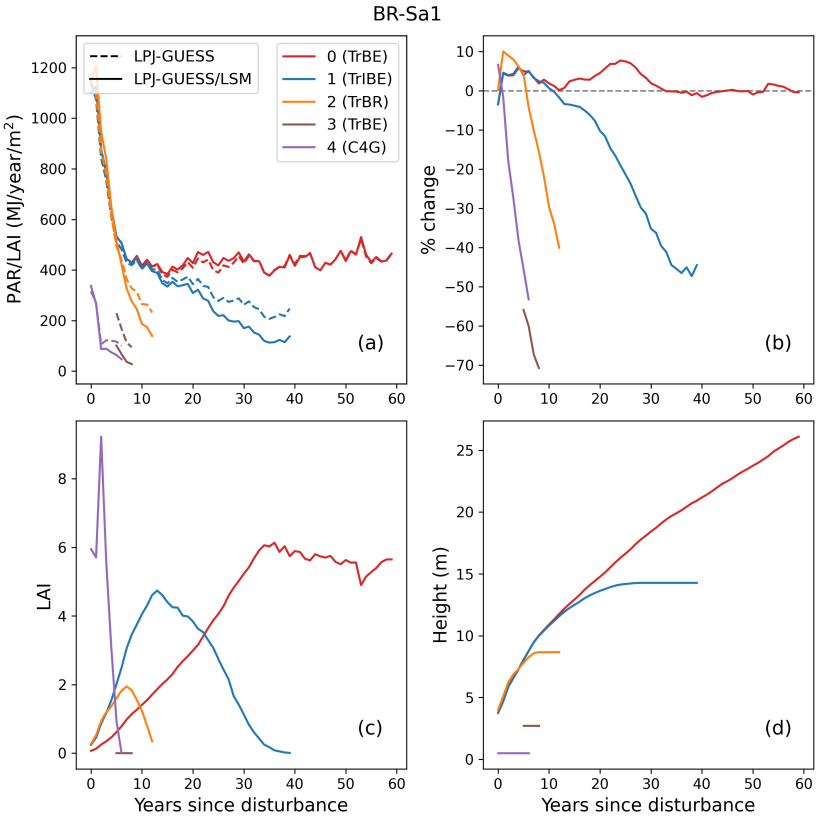

Figure 1: Comparison of PAR absorbed by the cohorts in a patch at BR-Sa1, calculated using the new radiative transfer scheme and the standard LPJ-GUESS PAR absorption scheme. *(a):* Annual absorbed PAR per leaf area; *(b):* Percent change in PAR absorption relative to standard LPJ-GUESS; *(c):* LAI; *(d):* Cohort height.

the tree cohorts have a lower leaf area index, so their leaves receive, on average, more direct sunlight than in the case of a thicker canopy. The new radiative scheme calculates higher values of absorbed PAR for these cohorts (panels *a* and *b*), and this feature dominates the overall difference between the two schemes in this site.

2 Spinup information

In a standard LPJ-GUESS simulation the 500-year spinup process proceeds as follows: the first 100 years, the model runs without nitrogen uptake to allow build up of soil nitrogen pools. All vegetation in the patch is then reset, and plant nitrogen uptake is turned on. Between years 140 and 220, information on the rates of change of C and N pools is collected. This information is then used

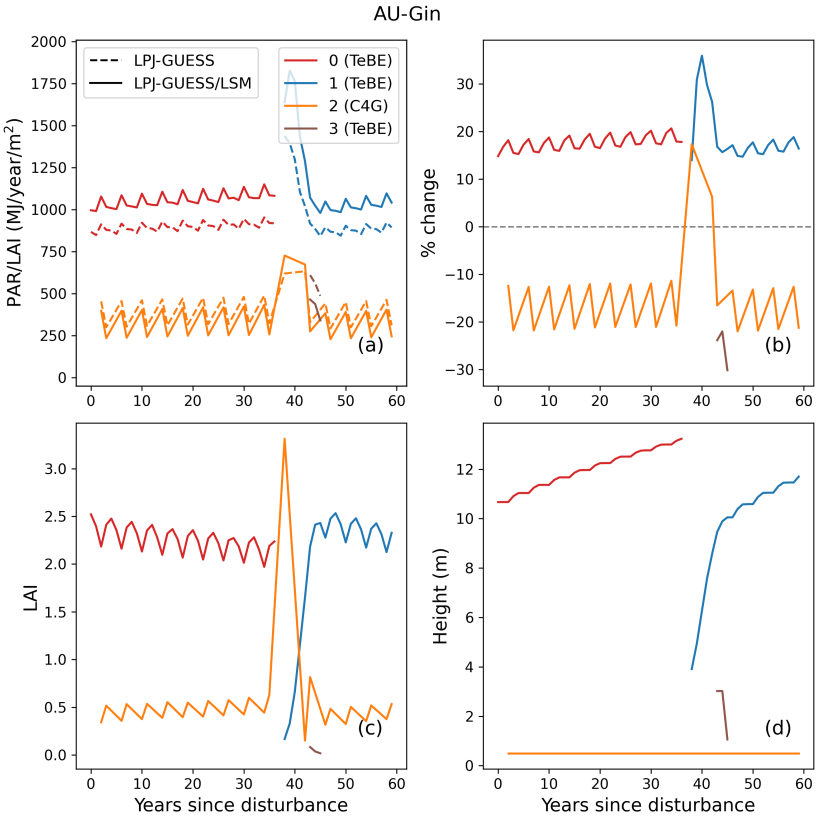

Figure 2: Comparison of PAR absorbed by the cohorts in a patch at BR-Sa1, calculated using the new radiative transfer scheme and the standard LPJ-GUESS PAR absorption scheme. *(a):* Annual absorbed PAR per leaf area; *(b):* Percent change in PAR absorption relative to standard LPJ-GUESS; *(c):* LAI; *(d):* Cohort height.

to calculate carbon and nitrogen steady-state pool sizes analitically, assuming an equilibration time of 40000 years for the soil organic matter pools. The model then runs for another 280 years, a period considered long enough for the vegetation C and N pools to reach steady state.

In general, the steady-state size of the carbon and nitrogen pools is determined by the balance between the rate of carbon input to the system (NPP) and the turnover rates of the soil organic matter pools. The LSM implementation changes the physical environment at which these processes take place in the model. Calculating photosynthesis rates at the newly simulated leaf temperature can lead to higher or lower carbon assimilation, depending on the PFT's optimal photosynthetic temperature range. It can also boost productivity by mitigating the effect of N limitation (see paper, Section 4.2). Soil organic matter decomposition is affected by soil temperature and humidity; higher (lower) tem-

	BB					Med				
	NPP	Temp	AWC	Soil C	Soil N	NPP	Temp	AWC	Soil C	Soil N
AU-Emr	-66.7	13.1	-30.0	-74.1	-74.1	-68.7	14.4	-49.6	-75.3	-75.3
ES-Amo	6.1	3.3	-11.6	-12.9	-12.9	0.6	3.7	-29.9	-12.9	-12.7
AU-DaP	1.8	4.5	46.2	-12.8	-10.2	25.5	4.4	19.8	21.7	25.7
AU-Stp	-42.8	8.5	-24.1	-50.5	-50.4	-23.0	9.0	-37.0	-33.6	-33.4
CG-Tch	87.6	2.5	51.5	6.8	9.2	92.0	1.8	52.1	10.4	12.9
PA-SPs	34.7	1.2	6.7	22.2	24.3	38.9	1.2	3.5	27.2	29.4
AU-DaS	-11.8	0.9	42.1	-0.9	3.5	-6.5	1.7	16.5	15.9	21.3
AU-Dry	-7.1	3.8	47.1	-2.0	1.0	1.4	3.3	11.8	4.5	6.5
SD-Dem	-13.1	-0.4	85.0	-45.9	-47.2	34.8	-0.3	-0.0	43.6	46.6
AU-Ade	-13.4	0.8	34.9	8.1	15.6	-8.7	0.8	16.6	21.4	29.5
AU-Gin	0.6	6.2	56.3	-32.7	-32.3	-9.1	6.0	25.7	-25.3	-23.6
AU-How	-13.8	-0.5	37.9	2.9	10.2	-10.6	-0.0	20.8	18.6	27.8
AU-RDF	4.6	3.3	45.4	15.0	19.9	12.0	3.6	21.0	28.7	33.1
AU-Rob	4.4	1.1	18.3	-6.4	-6.2	3.3	1.1	13.0	-2.1	-1.4
BR-Sa1	-25.2	-0.5	8.1	-16.0	-15.3	-20.5	-0.6	5.7	-14.2	-13.3
BR-Sa3	-11.1	-2.4	5.6	-8.7	-8.4	-6.2	-2.5	-3.2	-6.5	-6.3
GF-Guy	-14.6	0.3	9.9	-14.7	-14.5	-11.3	0.6	6.0	-12.6	-12.3
GH-Ank	-23.9	-0.3	13.3	-15.6	-13.4	-18.8	-0.7	11.4	-13.8	-11.5
MY-PSO	-30.1	0.3	59.2	-43.1	-42.6	-23.2	0.5	54.4	-37.5	-37.4
PA-SPn	-15.8	0.6	8.5	-20.6	-18.5	-12.1	0.7	5.5	-16.0	-13.6
ZM-Mon	-1.6	3.9	68.9	-18.1	-12.9	-3.8	1.8	39.5	-20.1	-15.3

Table 2: Percent change in steady-state NPP, average soil temperature over the top 50 cm of soil, average water content over the top 50 cm of soil, soil carbon content, and soil nitrogen content, relative to standard LPJ-GUESS. Steady state values are taken as the average of the last 100 years of spinup.

peratures and humidities lead to higher (lower) turnover rates. Table 2 shows a comparison of these factors in LSM and standard LPJ-GUESS simulations for all the sites considered in this study.

We show two examples of the build-up of the soil organic matter pools at BR-Sa1 (Fig. 3) and SD-Dem (Fig. 4), for the standard LPJ-GUESS, the CLM/BB, and the CLM/Med runs. At BR-Sa1 in the BB simulation, equilibrium NPP is lower than in standard LPJ-GUESS by $\sim 25\%$ (Table 2). Soil temperature is similar to standard LPJ-GUESS, but soil moisture is $\sim 8\%$ larger. This leads to lower equilibrium soil carbon ($\sim -16\%$) and nitrogen ($\sim -15\%$) content. The CLM/Med simulation behaves similarly at this site (and at most forest sites).

At SD-Dem the BB and Med simulations show very different behaviours. In the BB simulation, NPP is lower than in LPJ-GUESS, while the higher stomatal resistance given by the Ball-Berry scheme (see paper, Fig. 3) causes higher soil moisture content. This leads to lower equilibrium soil organic matter content values (a $\sim 46\%$ decrease compared to standard LPJ-GUESS). In the Med simulation, equilibrium NPP is substantially higher than in the standard LPJ-GUESS run, while lower soil moisture retention leads to slower decomposition rates, resulting in soil organic matter pools $\sim 44\%$ larger than in standard LPJ-GUESS.

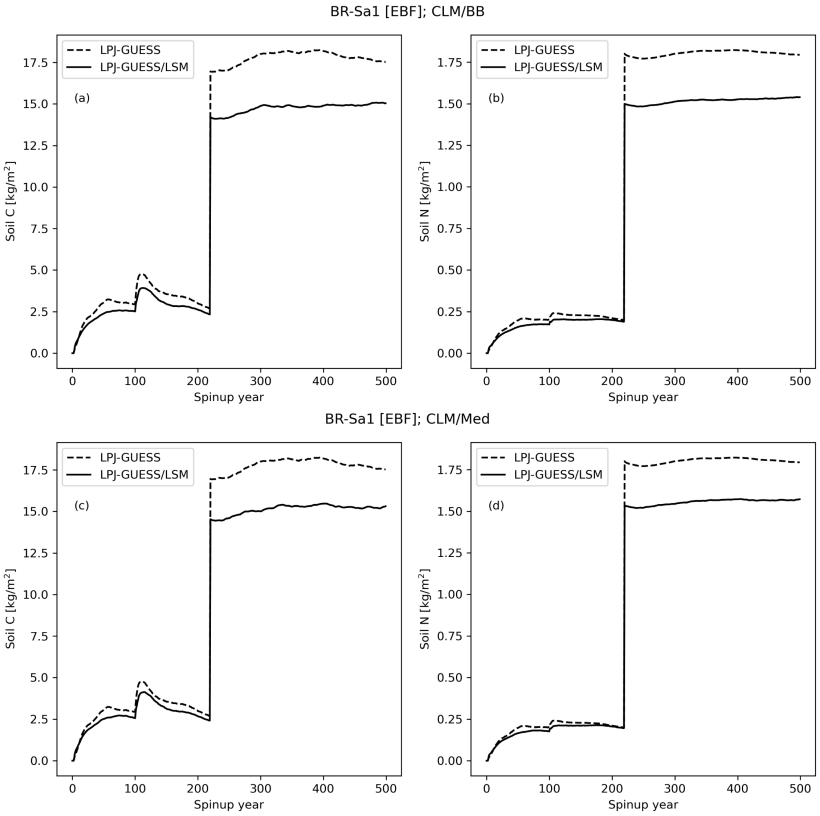

Figure 3: Comparison of the build up of carbon and nitrogen pools in the CLM/BB *(a) and (b)* and the CLM/Med *(c) and (d)* simulations with standard LPJ-GUESS, at BR-Sa1.

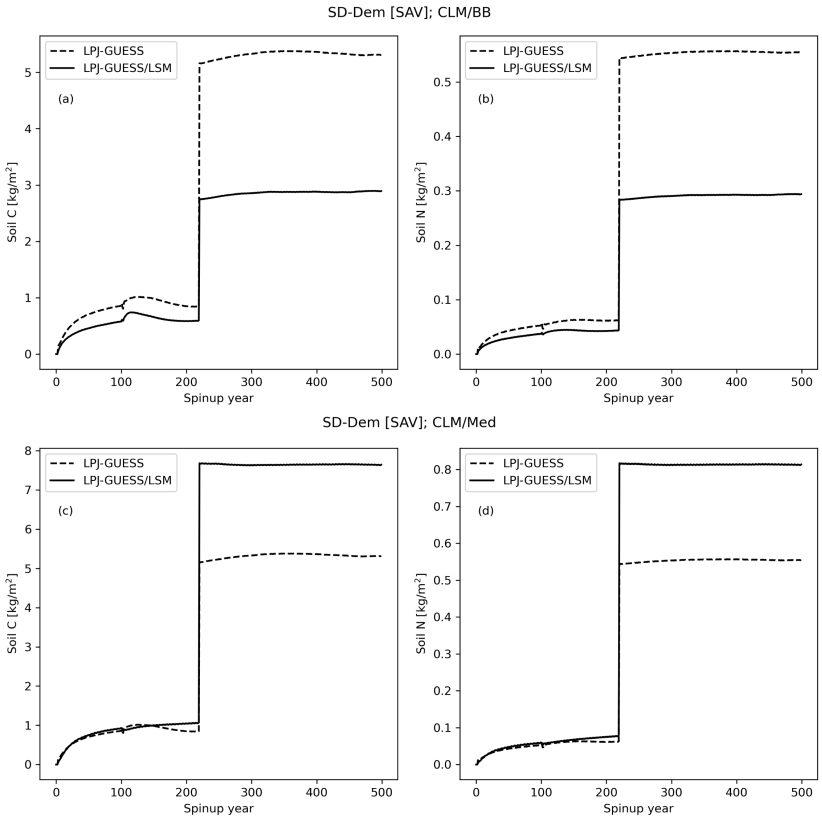

Figure 4: Comparison of the build up of carbon and nitrogen pools in the CLM/BB *(a) and (b)* and the CLM/Med *(c) and (d)* simulations with standard LPJ-GUESS, at SD-Dem.